Additive Manufacturing Innovations: Microstructure Optimisation for Ultra-High Silicon Electrical Steel Components

Rasoul Karami [1,2,3 a], David Butler [4,b], Yashar Javadi [1,5,c], Saeed Tamimi [1,2,3,d]

[1] Department of Design, Manufacturing and Engineering Management, University of Strathclyde, Glasgow, United Kingdom

[2]Advanced Forming Research Centre (AFRC), University of Strathclyde, Glasgow, United Kingdom

[3] National Manufacturing Institute Scotland (NMIS), University of Strathclyde, Glasgow, United Kingdom

[4] School of Engineering, University of Birmingham, Birmingham, United Kingdom

[5] Department of Electronics and Electrical Engineering, University of Strathclyde, Glasgow, United Kingdom

[a]rasoul.karami@strath.ac.uk, [b]d.l.butler@bham.ac.uk, [c]yashar.javadi@strath.ac.uk, [d]saeed.tamimi@strath.ac.uk

Abstract: The main objective of this work is to fabricate high-silicon electrical steel with an optimised microstructure for magnetic applications through additive manufacturing (AM) routes. Traditional thermomechanical manufacturing routes, such as hot and cold rolling operations, have struggled to produce non-oriented electrical steel (NGOES) components with more than 3.4 wt.% Si contents. However, the need for efficiency improvements requires an increase in silicon contents up to 6.5 wt.%, leading to compromised mechanical properties through conventional manufacturing techniques resulting in technical limitations on the production of these alloys. AM is a promising manufacturing approach that can address this challenge through near-net-shape fabrication. Optimisation process conditions in AM provide flexibility and enable better, more precise control over the microstructure. This study explores the microstructure and texture development of FeSi 6.5wt% NGOES using the laser metal deposition (LMD) technique. The influence of process parameters on microstructure has been investigated. The optimisation of the manufacturing process involved precise adjustments to processing parameters, specifically modifying the melt pool's shape and size by altering laser power and scanning speed during the process. The resulting fabricated samples exhibit elongated grain structures characterised by a strong <001>//BD fibre texture. Moreover, increasing laser energy density from 60 to 69.75 J/mm² enhances cube texture, improving NGOES magnetic properties. Higher laser power (400 to 465W) increases grain sizes, favouring <001> texture, highlighting the importance role of both energy density and laser power in shaping microstructure and texture of NGOES.

Keywords: additive manufacturing; microstructure; crystallographic texture; non-grain oriented electrical steel

Corresponding author: Rasoul Karami, email: rasoul.karami@strath.ac.uk

1. Introduction

Non-oriented grain electrical steel (NGOE) finds primary application as core material in various fields, including transformers, generators, and electric motors. This preference is due to its significant magnetic properties, including high permeability, saturation magnetization, low core loss, and cost-effectiveness [1]. For decades, ongoing research efforts have focused on enhancing the magnetic properties of NGOES through texture development. However, using conventional and traditional methods for optimising texture through cold rolling and annealing treatment were usually exhibiting a hard magnetic direction such as <111> known as (γ) and <110> known as (α) fibres, which is not desirable for magnetic properties. To improve the magnetic performance of NGOES, the desirable texture such as <001> (θ-fibre) known as an easy magnetic direction is required [1] . On the other side, NGOES with a high silicon content up to 6.5% demonstrate improved magnetic properties, including enhanced electrical resistivity and reduced magnetic anisotropy. These characteristics are desirable for improving the efficiency of electric motors in electric vehicles. However, with increasing silicon content, the formability of NGOES sheets decreases due to the formation of two brittle intermetallic phases, namely B_2 and DO_3 [2] which presents a limitation in the manufacturing process of these alloys using conventional methods. To address all these points, additive manufacturing (AM) provides numerous advantages. These include design freedom, material flexibility, precise control over processing parameters, and high solidification rate, all of which facilitate the desired microstructure and texture properties while minimising the occurrence of such phases in NGOES. As demonstrated in a prior study [3], parts with a composition of 6.9 wt% FeSi were manufactured using selective laser melting, resulting in the absence of these phases. This outcome can be attributed to the high cooling rate during processing, which effectively suppressed the formation of B2 and DO3 phases.

A uniform columnar grain shape in the building direction (BD) is highly desirable for FeSi, particularly for enhancing magnetic properties and texture along the <001> direction [1] , as well as for promoting Goss texture where the grains align with the magnetic flux directions [4]. However, there is considerable debate surrounding the optimal average grain size for enhancing the microstructure and texture of electrical steel. Some researchers have suggested a range between 50 to 150 μm [5], while others have supported for a size of 150μm [6, 7], 220μm [8], or even a broader range covering 536–615μm [9]. Despite these varied findings, significant uncertainty exists regarding the correct relationship between grain size and magnetic properties.

In addition to that, the microstructure and crystallographic texture of FeSi still require improvement to reduce core losses and enhance the magnetic permeability of NGOES thin sheets. A uniform columnar grain shape in the BD is desirable for FeSi, particularly for enhancing magnetic properties and texture along the <001> direction and Goss texture where the grains aligned with the magnetic flux directions. This alignment enables the orientation of magnetic moments in the BD, thereby maximising saturation magnetization. Additionally, it makes FeSi more responsive to magnetic fields in the BD and reduces hysteresis losses when grains are aligned in the BD, as the majority of domains are already aligned with the applied field direction, consequently reducing the energy required for alignment [10, 11]. Moreover, magnetic permeability is enhanced in the BD due to the alignment of grains, making it easier for FeSi materials to be magnetized by an applied magnetic field [12]. It has been reported that alternative AM processes such as laser metal deposition (LMD) Al-Mg alloy [13], Ti–6Al–4V [14], stainless steel 316L [15] offer a distinct advantage in the development of columnar grains aligned with the BD. This is attributed to significant thermal gradients and solidification behaviours during the process, which promote rapid nucleation, grain growth, and directional solidification. When higher energy input is applied, these conditions favour the formation of columnar grains aligned with the BD. Such grain structures have the potential to enhance magnetic properties and promote a favourable texture in NGOES sheets.

Hence, this study seeks to investigate how the LMD process contributes to the development of the desired microstructure and crystallographic texture in high-silicon electrical steel. Evaluation of the microstructure and texture evolution utilizes optical and electron microscopies. Furthermore, the

study examines the influence of LMD processing parameters, including laser power, scanning speed, and energy density, on the formation of the microstructure and texture.

2. Materials and experimental procedure

2.1 Sample processing

All samples in this study were manufactured from high silicon electrical steel gas-atomised powder (FeSi 6.5wt%) with a size range of 45-110 μm with a mean particle size of 77.5 μm, a Hall flowmeter measurement of 19.0 s/50g, and an apparent density of 4.06 g/cm³ supplied by MSE Supplies LLC company. The chemical composition of NGOES used in this study is (wt%: 92.9 Fe, 6.6 Si, Al 0.46, 0.005 C, 0.005 S, 0.009 O, 0.004 N) with size distribution of D10: 34.5 μm, D50: 78.5 μm, D90:116 μm. Hybrid LMD technologies were utilised, incorporating a 3+2 axis CNC Milling machine, a 1.5kW Ytterbium Fiber laser, and localised argon shielding from a nozzle. In this investigation, only localized shielding was employed for depositing thin walls measuring 20 * 30 * 1.5 mm³ to examine microstructure and crystallographic texture. A 1 mm spot size and a powder feed rate of 2.5 g/min were maintained for all depositions. The spacing between scan track centrelines within each layer, referred to as tracking space or hatch space for foundation layers, was set at 0.6 mm horizontally, while the vertical distance or thickness between each layer, known as z-step along the BD, remained fixed at 0.45 mm. The samples were processed with a variety of processing parameters such as laser power (P:400 to 465W), scan speed (V:380 to 440mm/sec), energy density (E:60 to 69.75 J/mm^2). The X axis is also referred to as the BD and samples were removed by wire electrical-discharge machining due to their size, precision cutting, and the minimal mechanical stress that can be achieved in this cutting process.

2.2 Sample preparation, optical microscopy and EBSD

Thin-wall samples were prepared for both optical microscopy and EBSD by hot mounting, followed by grinding and polishing. To assess microstructure features, optical micrographs were taken of the XY plane using Hirox and Leica microscopes. The samples were retained in Bakelite for EBSD analysis. EBSD analysis was performed utilizing a FEI Quanta 650 scanning electron microscope equipped with an Oxford Instruments Symmetry EBSD detector. The analysis was conducted at an accelerating voltage of 25 kV with a step size of 3 μm, and the sample was tilted 70 degrees to the laser beam. EBSD data was captured using the Aztec software by Oxford Instruments, with FeSi 6.5 wt.% indexed based on the library parameters for α-iron body centred cubic (BCC). Singular phase detection was achieved with an indexing rate exceeding 99%.

3. Results and discussion

3.1 Microstructure evolution during LMD of FeSi 6.5wt%

The microstructure of as-deposited LMD FeSi 6.5wt% was examined to better understand the changes in microstructure that occur throughout the LMD process. As it can be seen in Figure 1 microstructure consisted of columnar grains up to several millimetres in length aligned in the BD. However, fine equiaxed were observed after first, and last layers as well as some area in long edges of FeSi 6.5wt% deposited. This behaviour is also observed in development of texture NGOES steel [16]. This observation is primarily due to a substantial temperature gradient within the melt pool, resulting in a rapid growth of columnar grains and decreasing the likelihood of new sites nucleating during the solidification process. Additionally, it can be observed that fine grains nucleated and formed at first layer, along the long edges, and at the last layer possibly due to the substrate acting as a thermal sink when the first layer of FeSi was deposited and being exposed to the atmosphere on both side (along edges) and three sides (top) of the samples cause to increase cooling rate and forming fine grains at these areas. This strategy exposes these areas to less laser time, resulting in lower heat accumulation due to the laser's travel time, thus promoting the development of new fine grains.

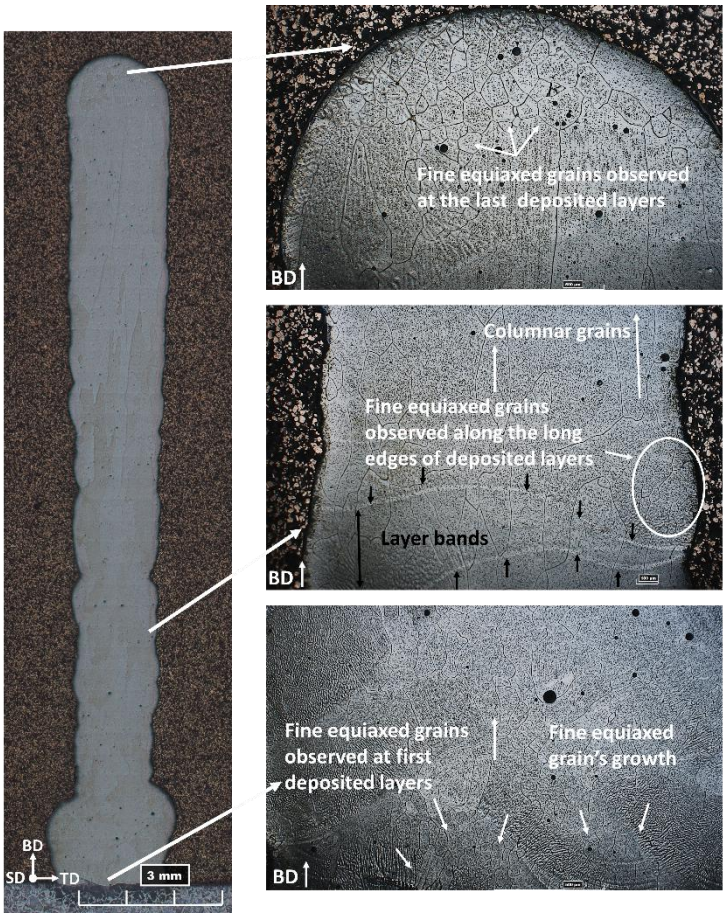

Figure 1. The optical graph of etched specimen consisting of different sections of the sample.

It is worth mentioning that optimising processing parameters such as appropriate laser power during the AM process can avoid defects such as keyholing and porosity at the bottom of melt pool [17]. It is desirable that to have melt pool in conduction mode with no defects such as entrapped gas porosity and keyholes. However, at high laser power, it is likely these types of defects will be present due to turbulence in the melt pool [18]. Characteristics of the melt pool such as thermal phenomena as well as heat transfer (conduction, convection, radiation) are key players in the stability of the melt pool during the additive manufacturing process [1, 19]. The schematic of the thermal phenomena, melt boundary, and columnar grain development of FeSi 6.5wt% during the LMD process can be seen in Figure 2.

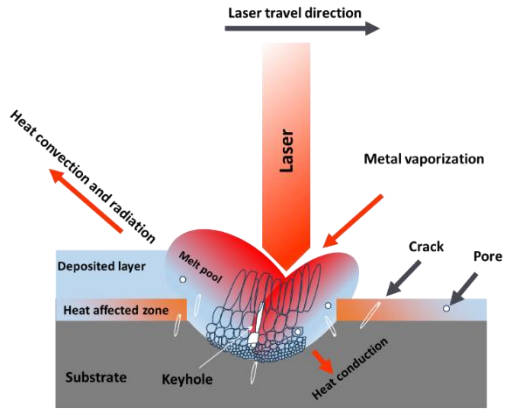

Figure 2. Schematic of melt pool boundary, thermal phenomena and columnar grain development occurring during LMD process.

To investigate and understand the evolution behaviour of the microstructure during the layer-by-layer deposition process in the LMD process, an optical macrograph image has been obtained with

the layer bands, as shown in Figure 3. In this case, the melt pool size is notably large as observed in [20], primarily resulting from the high laser power's influence in the LMD process. This effect outweighs other factors such as feed rate and powder mass flow. Additionally, the melt pool size is further increased due to the preheating of the substrate. According to [21] preheating will lead to an increase in melt pool depth in conduction area and resulting in a larger melt pool. Furthermore, as depicted in Figure 1 and Figure 3 numerous layer bands are observed, similar to the reported findings of [22] and [23]. This observation may be attributed to the superheating effect, which initiates melting in the previous layer's pool, forming a narrow band with a temperature exceeding the solidus temperature. However, due to limited time, the material remains in the solid phase. As can be seen in Figure 3

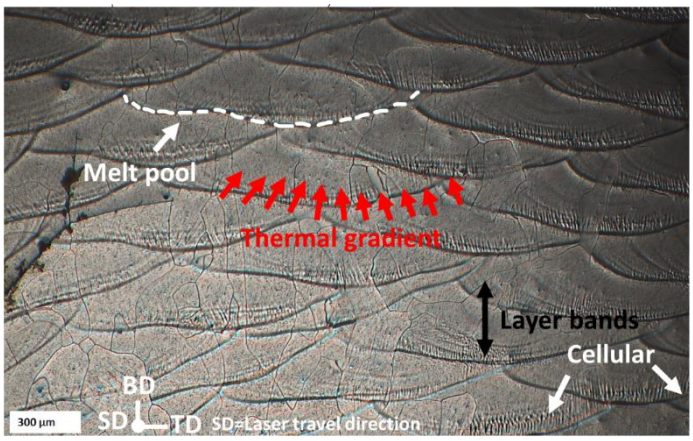

Figure 3 the formation of a shallow melt pool with a curved surface occurs during the LMD process, where the melt pool is in motion. Additionally, the solidification substructure predominantly develops parallel to the BDthe BD and due to high thermal gradient, which is perpendicular to the melt pool, and it is noticeable, in this case that the melt pool is tilted towards the laser movement. Overall, this caused the growth of preferential direction grains of {001}mainly in the BD which will be covered in more detail in the EBSD case studies in section 3.2 [24].

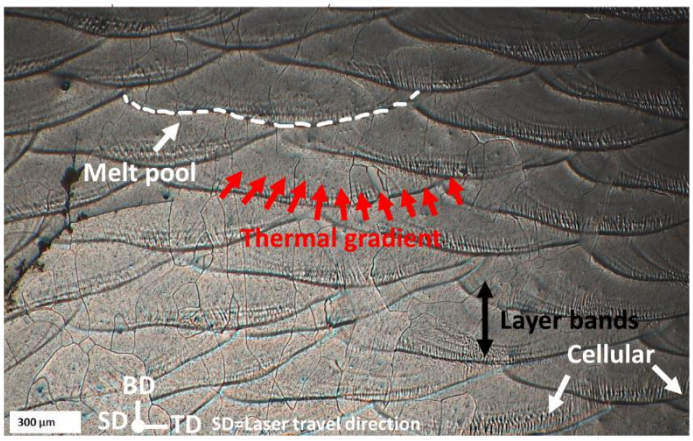

Figure 3. Optical graph of the direction of maximum thermal gradient with respect to the melt pool geometry.

It is worth mentioning that defects such as pores can be detrimental for microstructure development. It is possible that pores can act as a thermal sink and absorb all heat provided by the laser not allowing the heat to distribute through the normal conduction across the sample and cause the temperature to rise in the melt pool Figure 4. This abnormal temperature in the melt pool led to the formation of two different areas of equiaxed and elongated grains. At the tip of the pore, equiaxed grains form due to the presence of an air gap that blocks heat conduction distribution. This lack of a heat source and higher cooling rate contribute to the formation of smaller grains. Also, in the

absence of defects, the above equiaxed grains, due to higher heat input, rapidly change in temperature across the sample, and directional solidification inherent in LMD, the grain starts to grow in specific direction and leading elongated grain structures.

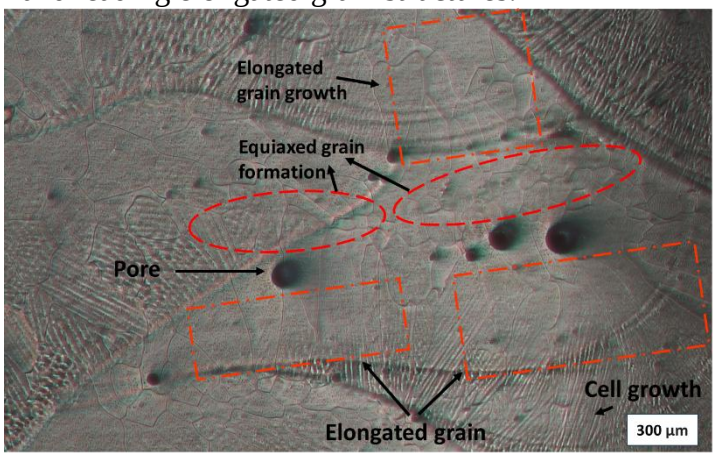

Figure 4. Effect of pore on microstructural development.

During the solidification process in BCC materials such as FeSi, as materials transition from a liquid to a solid state, it is easy for atoms to stick to the less closely packed planes such as {001} due to their low energy configurations. These planes have favourable orientations for the growth of crystals <001> and become more prominent during solidification process [25]. As can be seen in Figure 5 the schematic illustrates the development of crystal orientation <001> in the BD for high silicon electrical steel 6.5 wt% deposited by the LMD process. This phenomenon was also reported in other AM research [3, 15] where grains with preferred crystal growth direction such as <001> formed along the BD compared to other weakly oriented grains. This alignment occurs because it closely follows the thermal gradient direction where rapid solidification happens. In other words, the grains with <001> direction aligned more closely to the vertical thermal gradient direction which is the BD and these preferred grains orientation grow easily and dominate. Since epitaxial growth requires minimal undercooling to occur, cellular and columnar grains grow in an epitaxial manner from the substrate grain and creating a columnar grain growing perpendicular in the BD during directional solidification phenomenon [26].

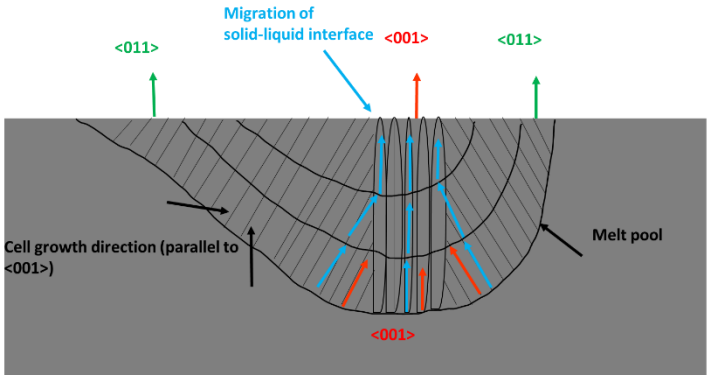

Figure 5. Development of crystal orientation <001> in build direction of FeSi 6.5 wt% deposited by LMD process

3.2 Effect of laser power on <001> texture development

FeSi 6.5wt% was manufactured using the LMD process. EBSD was conducted on the XY plane for all samples. The obtained EBSD map was utilised to analysis the crystallographic texture of LMD-manufactured high silicon electrical steel (6.5wt%) in the BD-TD plane and confirm the presence of the <001> texture in the BD. As can be seen in Figure 6, the EBSD map of two different samples TW1 (a) and TW2 (b) with energy densities of 60 and 69.75 J/mm$^{\wedge 2}$, respectively. This illustration indicates that the samples contain a <001> texture along the BD direction, as well as columnar grains. Moreover, the EBSD maps of samples TW1 (P:400W, V:400mm/sec) and TW2 (P:465W, V:400mm/sec) aim to provide an overview of the correlation between grain morphology,

energy density, and <001> texture along the BD. As it can be seen for sample TW2 the front view showed that majority of the long columnar grains preferentially orient their axes along the BD. This result illustrates the hypothesis of epitaxial grain growth along the BD direction as the laser energy density increased from 60 to 69.75 J/mm^2. Hence, in TW1, a smaller portion of the grains appears red compared to TW2 due less deviation along the BD as laser energy density increased. This suggests that varying energy density inputs during FeSi deposition can induce differences in heat distribution and cooling rates within the materials, consequently resulting in different thermal gradients across the deposited materials. These variations can significantly impact the microstructure and texture of FeSi parts [27, 28]. The dependency of crystallographic texture intensities and morphology on laser energy input in direct energy deposition processes like LPBF has been reported in research studies [3, 29-31]. These studies revealed that not only does increasing laser energy density lead to elongated grains, but also increasing the size of the melt pool causes the <001> fibre texture to shift towards a cube texture. In other words, increasing laser power from 400 to 465W causes a larger melt pool and partially remelted grains with crystallographic direction of <001> along the BD which can serve as a foundation for the newly process materials to solidify in an epitaxial manner. This results in enlarged oriented grains as well as stronger texture intensities.

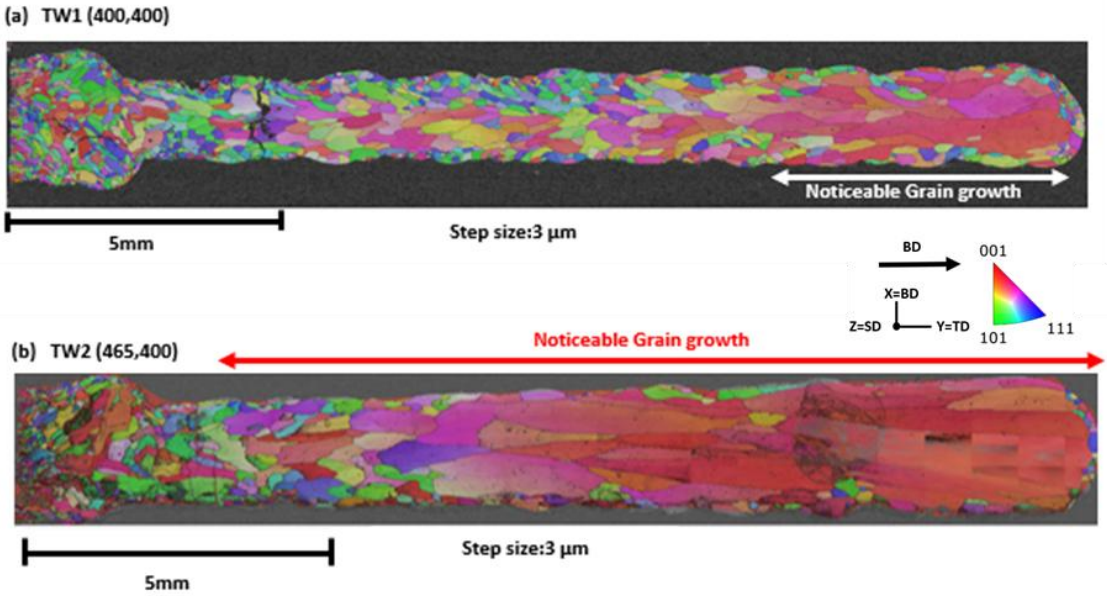

Figure 6. EBSD maps (a and b) and IPFs for TW1 and TW2 in build directions.

The orientation distribution functions (ODFs) of the scanned areas are presented in

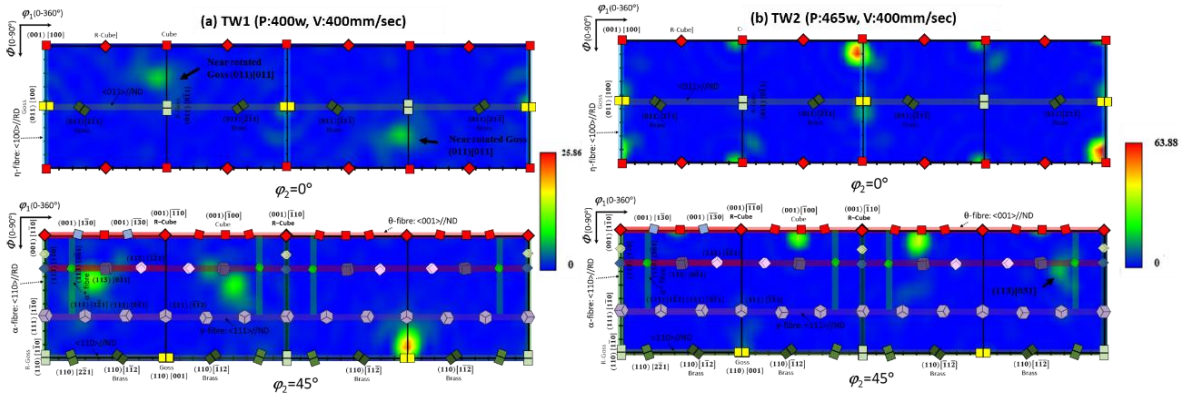

Figure 7. While all samples exhibited texture, significant differences were observed in both the type and intensity among them. As the laser power increases from 400 to 465W, while maintaining a constant scan speed of 400 mm/sec, the intensity of the texture also increases, rising from 26 of a random distribution (MRD), to a maximum intensity of 64 MRD. In the ODF section

φ_2 = 0°, with the increase in laser energy to 465W, the components Goss texture (001)[100] and near rotated Goss texture (011)[0$\bar{1}$1] transition to a significantly strong cube texture. Additionally, in the ODF section φ_2 = 45°, as the laser energy reaches 465W, texture components close to (113)[1$\bar{2}$1] and Goss (110)[001] transform into a strong cube texture (001)[100], and with a weak texture of (113)[0$\bar{3}$1]. Notably, there is an absence of <111>//BD (γ-fibre) or <110>//RD (α-fibre) orientations, which are detrimental to the magnetic properties of high silicon electrical steel. It can be concluded that the texture is predominantly dominated by a cube texture which is ideal texture for NGOES used as core lamination for electric motors. It is noteworthy that producing this cube texture poses significant challenges in electrical steels through conventional rolling and annealing methods, particularly when the steel composition exceeds 3.4wt% Si [6, 32]. However, utilizing LMD offers a viable solution to achieve this desired texture.

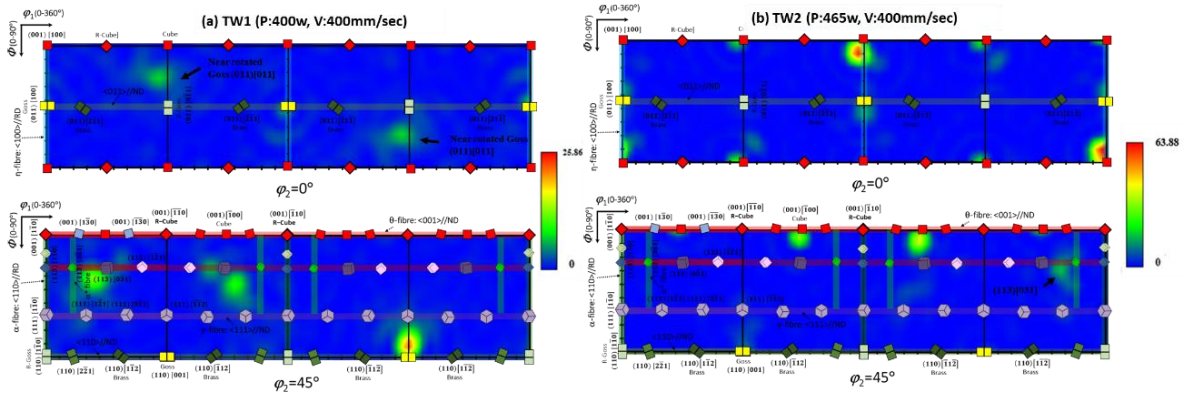

Figure 7.Macrotexture of FeSi 6.5wt% shown on φ2 = 0° and 45° ODF sections for sample TW1 (a) and sample TW2 (b).

3.3 Effect of laser power on grain size evolution

The effect of the laser power on grain development of FeSi 6.5wt% was investigated. To have a representative value for overall grains size, the weighted average equivalent circle diameter was used to measure the average grain size. The results show that by increasing laser power from 400 to 465 W, the weighted average equivalent circle diameter increased by approximately 220% (from 500 to above 1600 µm) Figure 8.

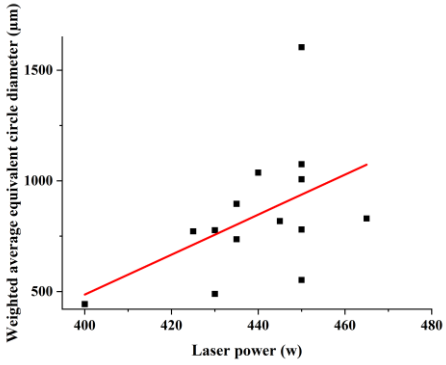

Figure 8. Effect of the laser power on grain size.

Several factors contribute to the increase in grain size, especially in the LMD process. One such factor is the high thermal gradient experienced by the metal during rapid heating and cooling, affecting grain nucleation and growth. This phenomenon results in larger grain sizes, particularly in areas where heat accumulates, as noted in the BD [33]. Adjusting the thermal gradient during the manufacturing process, as suggested in [34], can alter the texture, while increasing laser energy density can lead to intensify <001> texture. Additionally, the solidification rate plays a crucial role in influencing grain size. For instance, altering the local solidification conditions by adjusting the building orientation can influence the morphology of grains, leading them to become either equiaxed (smaller) or columnar (larger). In simpler terms, changing the solidification process can modify the appearance of grains, a characteristic closely tied to the undercooling conditions.

Undercooling, in turn, depends on the thermal gradient (G) and the rate of solidification interface movement between solid and liquid (R). Consequently, a low (G/R) ratio results in increased undercooling, which is advantageous for forming equiaxed solidification morphology [35]. Moreover, as the solidification rate decreases, there is more time for atoms to migrate and form larger grains, resulting in coarser and larger grain sizes [36]. In this scenario, a high thermal gradient and rapid solidification have led to the formation of columnar grains along the BD, aligned with the heat flow. Consequently, the combination of these factors not only promotes the elongation of grains but also contributes to an increase in grain size.

Also according to [37] residual stress induced during the LMD process also impacts the microstructure. In regions with higher residual stress, preferential grain growth may occur such as <001>, leading to larger grain sizes. However, contrasting results were reported by [38] where the small grains formed when there is low residual stress existing. Additionally, process parameters like laser energy density can influence the thermal profile and cooling rate, consequently affecting the formation of columnar grains on the side and top planes. This can also lead to an increased depth of the molten pool and a transition from a crystallographic <001> fibre texture to a cube texture [3, 29]. Thus, laser energy density plays a crucial role in the microstructural evolution, particularly in grain growth during the LMD processes. For example, as can be seen in

Figure 9

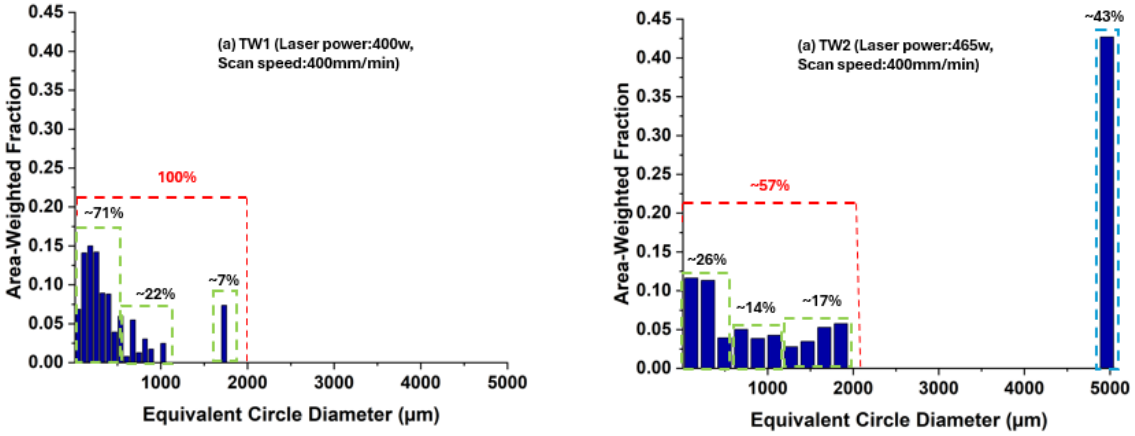

Figure 9 (a) and (b) provided bar charts compare two samples, TW1 and TW2, in terms of grain size distribution and the effects of different laser power settings used in their preparation. Sample TW1, prepared with a laser power of 400W and a scan speed of 400mm/min, illustrates a grain size distribution predominantly within the 0 to 2000 μm range. Specifically, approximately 71% (area weighted fraction) of the grains fall within the 0 to 500 μm range, 22% between 500 to 1000 μm, and 7% between 1000 to 2000 μm. This indicates a narrow grain size distribution with negligible grains beyond 2000 μm. In contrast, sample TW2, prepared with a higher laser power of 465W but the same scan speed of 400mm/min, exhibits a broader and more varied grain size distribution. In TW2, about 26% of the grains are within the 0 to 500 μm range, 14% between 500 to 1000 μm, 17% between 1000 to 2000 μm, and a significant 43% at the 5000 μm mark. This indicates the presence of much larger grains in TW2 compared to TW1. The comparison highlights that the increase in laser power from 400W in TW15 to 465W in TW2 results in a substantial shift in grain size distribution. TW2 shows a reduction in the fraction of smaller grains (0 to 500 μm) from 71% to 26%, a decrease of approximately 63.4%, and an increase in the proportion of larger grains (5000 μm) to 43%, compared to none in TW1. In other words, by increasing the energy density, the grain size increased by 177.78%. This notable grain growth is also apparent in Figure 6

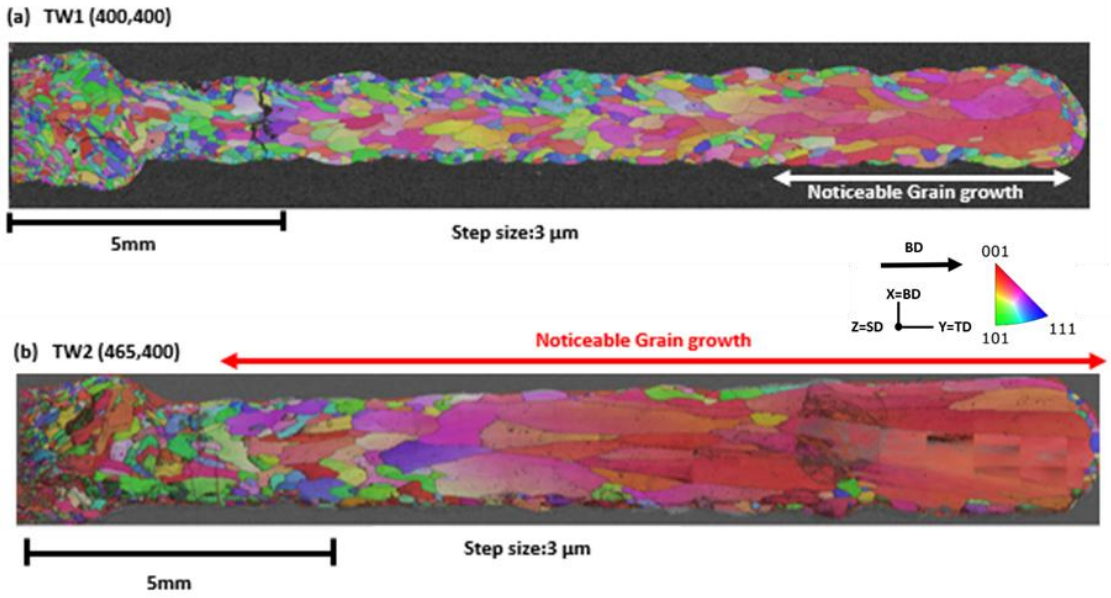

Figure 6. EBSD maps (a and b) and IPFs for TW1 and TW2 in build directions.

. These findings highlight the influence of higher laser power on promoting larger grain growth, leading to a broader and coarser grain size distribution in Sample TW2.

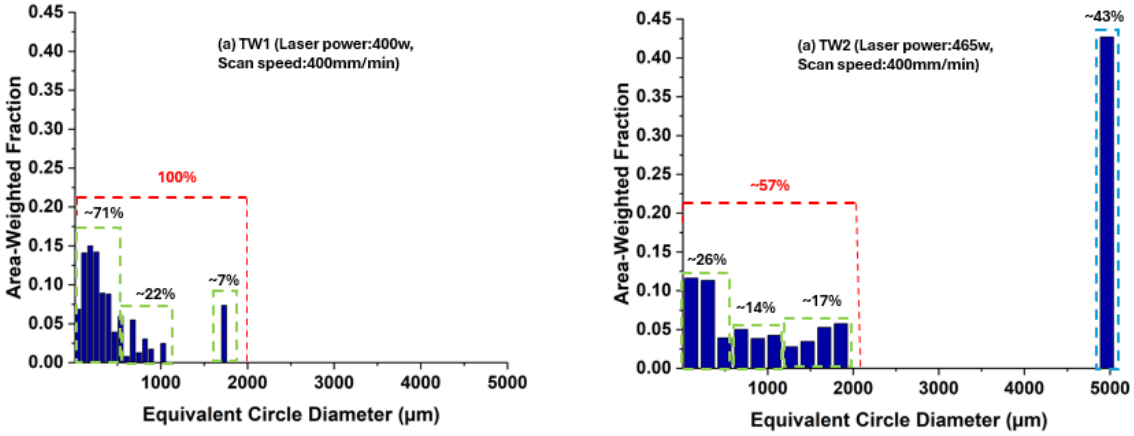

Figure 9. Grain development based on area weighted fraction of different samples (a) TW1, (b) TW2.

4. Conclusion

Based on the detailed investigation into the microstructure and crystallographic texture evolution of FeSi 6.5wt% using LMD, several key findings emerge. Firstly, the LMD process, coupled with varying laser power, scan speed, and energy density, demonstrates significant influence over the microstructure and texture development of high silicon electrical steel. Through careful optimisation of these parameters, it is possible to tailor the microstructural characteristics to achieve desired properties. The analysis reveals a strong correlation between laser power and the development of <001> texture along the BD. Increasing laser energy density from (60 to 69.75 J/mm^2) promotes a more intense texture, with a notable shift towards cube texture, which is desirable for enhancing the magnetic properties of NGOES. This highlights the importance of precise control over processing parameters in achieving the desired crystallographic orientation. Furthermore, the investigation into grain size evolution reveals the complex relationship between thermal gradients, solidification rates during the LMD process. Increased laser power from 400 to 465 W leads to increased grain sizes, with larger grains favouring the formation of <001> texture. This highlights the critical role of energy density in dictating microstructural characteristics and texture evolution.

Overall, these findings underline the potential of LMD technology in advancing the microstructure and texture of high silicon electrical steel, offering opportunities for enhanced magnetic properties and improved performance in applications such as transformers, generators, and electric motors. By further refining our understanding of the complex relationships between processing parameters and material properties, we can unlock new avenues for optimising the performance of electrical steel in various industrial applications.

References

[1] R. Karami, D. Butler, and S. Tamimi, "Manufacturing of non-grain-oriented electrical steels: review," *The International Journal of Advanced Manufacturing Technology*, 2024/06/04 2024, doi: 10.1007/s00170-024-13837-9.

[2] C. Li, G. Cai, B. Cai, and Q. Wang, "Impact of rolling temperature on microstructure, ordered phases, and ductility in Fe–6.5 wt% Si magnetic material," *Journal of Materials Research*, vol. 31, no. 19, pp. 3004-3015, 2016.

[3] M. Garibaldi, I. Ashcroft, M. Simonelli, and R. Hague, "Metallurgy of high-silicon steel parts produced using Selective Laser Melting," *Acta Materialia*, vol. 110, pp. 207-216, 2016/05/15/ 2016, doi: https://doi.org/10.1016/j.actamat.2016.03.037.

[4] H. Williams, "Magnetic properties of single crystals of silicon iron," *Physical Review*, vol. 52, no. 7, p. 747, 1937.

[5] Y. Hayakawa, "Electrical Steels," 2020.

[6] S. Tamimi *et al.*, "Mechanical properties and crystallographic texture of non-oriented electrical steel processed by repetitive bending under tension," *Materials Science and Engineering: A*, vol. 835, p. 142665, 2022/02/17/ 2022, doi: https://doi.org/10.1016/j.msea.2022.142665.

[7] M. Shiozaki and Y. Kurosaki, "The effects of grain size on the magnetic properties of nonoriented electrical steel sheets," *Journal of materials engineering*, vol. 11, no. 1, pp. 37-43, 1989.

[8] A. B. Kustas, S. Chandrasekar, and K. P. Trumble, "Magnetic properties characterization of shear-textured 4 wt% Si electrical steel sheet," *Journal of Materials Research*, vol. 31, no. 24, pp. 3930-3938, 2016.

[9] H. Pan, Z. Zhang, and J. Xie, "The effects of recrystallization texture and grain size on magnetic properties of 6.5wt% Si electrical steel," *Journal of Magnetism and Magnetic Materials*, vol. 401, pp. 625-632, 2016/03/01/ 2016, doi: https://doi.org/10.1016/j.jmmm.2015.10.047.

[10] K. M. Lee, S. Y. Park, M. Y. Huh, J. S. Kim, and O. Engler, "Effect of texture and grain size on magnetic flux density and core loss in non-oriented electrical steel containing 3.15% Si," *Journal of Magnetism and Magnetic Materials*, vol. 354, pp. 324-332, 2014/03/01/ 2014, doi: https://doi.org/10.1016/j.jmmm.2013.11.030.

[11] V. M. Paltanea, G. Paltanea, H. Gavrila, and L. Dumitru, "Experimental analysis of magnetic anisotropy in silicon iron steels using the single strip tester," in *2015 9th International Symposium on Advanced Topics in Electrical Engineering (ATEE)*, 2015: IEEE, pp. 456-459.

[12] G. Stornelli *et al.*, "Properties of additively manufactured electric steel powder cores with increased Si content," *Materials*, vol. 14, no. 6, p. 1489, 2021.

[13] M. Froend, V. Ventzke, F. Dorn, N. Kashaev, B. Klusemann, and J. Enz, "Microstructure by design: An approach of grain refinement and isotropy improvement in multi-layer wire-based laser metal deposition," *Materials Science and Engineering: A*, vol. 772, p. 138635, 2020/01/20/ 2020, doi: https://doi.org/10.1016/j.msea.2019.138635.

[14] C. Selcuk, "Laser metal deposition for powder metallurgy parts," *Powder Metallurgy*, vol. 54, no. 2, pp. 94-99, 2011.

[15] R. W. Fonda and D. J. Rowenhorst, "Crystallographic Variability in Additive Manufacturing," in *IOP Conference Series: Materials Science and Engineering*, 2022, vol. 1249, no. 1: IOP Publishing, p. 012007.
[16] J.-T. Park and J. A. Szpunar, "Effect of initial grain size on texture evolution and magnetic properties in nonoriented electrical steels," *Journal of Magnetism and Magnetic Materials*, vol. 321, no. 13, pp. 1928-1932, 2009/07/01/ 2009, doi: https://doi.org/10.1016/j.jmmm.2008.12.015.
[17] J. Li, L. Cao, J. Xu, S. Wang, and Q. Zhou, "In situ porosity intelligent classification of selective laser melting based on coaxial monitoring and image processing," *Measurement*, vol. 187, p. 110232, 2022/01/01/ 2022, doi: https://doi.org/10.1016/j.measurement.2021.110232.
[18] P. Akbari *et al.*, "MeltpoolNet: Melt pool characteristic prediction in Metal Additive Manufacturing using machine learning," *Additive Manufacturing*, vol. 55, p. 102817, 2022/07/01/ 2022, doi: https://doi.org/10.1016/j.addma.2022.102817.
[19] J. Wang, R. Zhu, Y. Liu, and L. Zhang, "Understanding melt pool characteristics in laser powder bed fusion: An overview of single- and multi-track melt pools for process optimization," *Advanced Powder Materials*, vol. 2, no. 4, p. 100137, 2023/10/01/ 2023, doi: https://doi.org/10.1016/j.apmate.2023.100137.
[20] S. Ocylok, E. Alexeev, S. Mann, A. Weisheit, K. Wissenbach, and I. Kelbassa, "Correlations of Melt Pool Geometry and Process Parameters During Laser Metal Deposition by Coaxial Process Monitoring," *Physics Procedia*, vol. 56, pp. 228-238, 2014/01/01/ 2014, doi: https://doi.org/10.1016/j.phpro.2014.08.167.
[21] Q. Chen *et al.*, "Elucidating the effect of preheating temperature on melt pool morphology variation in Inconel 718 laser powder bed fusion via simulation and experiment," *Additive Manufacturing*, vol. 37, p. 101642, 2021/01/01/ 2021, doi: https://doi.org/10.1016/j.addma.2020.101642.
[22] Y. Zhu, X. Tian, J. Li, and H. Wang, "Microstructure evolution and layer bands of laser melting deposition Ti–6.5 Al–3.5 Mo–1.5 Zr–0.3 Si titanium alloy," *Journal of Alloys and Compounds*, vol. 616, pp. 468-474, 2014.
[23] A. Ho, H. Zhao, J. W. Fellowes, F. Martina, A. E. Davis, and P. B. Prangnell, "On the origin of microstructural banding in Ti-6Al4V wire-arc based high deposition rate additive manufacturing," *Acta Materialia*, vol. 166, pp. 306-323, 2019/03/01/ 2019, doi: https://doi.org/10.1016/j.actamat.2018.12.038.
[24] T. DebRoy *et al.*, "Additive manufacturing of metallic components–process, structure and properties," *Progress in Materials Science*, vol. 92, pp. 112-224, 2018.
[25] S. Suwas and R. K. Ray, *Crystallographic texture of materials*. Springer, 2014.
[26] S. Kou, "Welding metallurgy," *New Jersey, USA*, vol. 431, no. 446, pp. 223-225, 2003.
[27] J. Li, H. Ren, C. Liu, and S. Shang, "The effect of specific energy density on microstructure and corrosion resistance of CoCrMo alloy fabricated by laser metal deposition," *Materials*, vol. 12, no. 8, p. 1321, 2019.
[28] X. Shen, F. Meng, K. B. Lau, P. Wang, and C. H. T. Lee, "Texture and microstructure characterizations of Fe-3.5wt%Si soft magnetic alloy fabricated via laser powder bed fusion," *Materials Characterization*, vol. 189, p. 112012, 2022/07/01/ 2022, doi: https://doi.org/10.1016/j.matchar.2022.112012.
[29] M. Garibaldi, I. Ashcroft, N. Hillier, S. A. C. Harmon, and R. Hague, "Relationship between laser energy input, microstructures and magnetic properties of selective laser melted Fe-6.9%wt Si soft magnets," *Materials Characterization*, vol. 143, pp. 144-151, 2018/09/01/ 2018, doi: https://doi.org/10.1016/j.matchar.2018.01.016.
[30] F. Meng *et al.*, "Texture components and magnetic properties of laser powder bed fusion fabricated near grain-oriented and near non-oriented silicon steel," *Materials & Design*, vol. 231, p. 112037, 2023/07/01/ 2023, doi: https://doi.org/10.1016/j.matdes.2023.112037.

[31] T. Niendorf, S. Leuders, A. Riemer, H. A. Richard, T. Tröster, and D. Schwarze, "Highly anisotropic steel processed by selective laser melting," *Metallurgical and materials transactions B*, vol. 44, pp. 794-796, 2013.
[32] Y. He, E. Hilinski, and J. Li, "Texture evolution of a non-oriented electrical steel cold rolled at directions different from the hot rolling direction," *Metallurgical and Materials Transactions A*, vol. 46, pp. 5350-5365, 2015.
[33] A. R. A. Dezfoli, W.-S. Hwang, W.-C. Huang, and T.-W. Tsai, "Determination and controlling of grain structure of metals after laser incidence: Theoretical approach," *Scientific reports*, vol. 7, no. 1, p. 41527, 2017.
[34] Z. Lin *et al.*, "Crystallographic Texture Control of Niti Alloy by Adjusting the Thermal Gradient of Laser Powder Bed Melting," *Available at SSRN 4745122*.
[35] M. Sanjari *et al.*, "Microstructure, texture, and anisotropic mechanical behavior of selective laser melted maraging stainless steels," *Materials Characterization*, vol. 192, p. 112185, 2022/10/01/ 2022, doi: https://doi.org/10.1016/j.matchar.2022.112185.
[36] C. Bernauer, M. E. Sigl, S. Grabmann, T. Merk, A. Zapata, and M. F. Zaeh, "Effects of the thermal history on the microstructural and the mechanical properties of stainless steel 316L parts produced by wire-based laser metal deposition," *Materials Science and Engineering: A*, vol. 889, p. 145862, 2024/01/01/ 2024, doi: https://doi.org/10.1016/j.msea.2023.145862.
[37] M. R. Borhani, M. Rajabi, R. S. Razavi, and R. Jamaati, "Investigating the relationship between mechanical properties and residual stress in the laser cladding process of Inconel 625 superalloy," *Heliyon*, vol. 9, no. 9, 2023.
[38] X. Zou, Z. Yan, K. Zou, S. Gang Zhang, W. Liu, and L. Song, "Residual stress control of 316 L stainless steel using pulsed-wave laser additive manufacturing," *Optics & Laser Technology*, vol. 150, p. 107910, 2022/06/01/ 2022, doi: https://doi.org/10.1016/j.optlastec.2022.107910.